ACS Photonics

Article

pubs.acs.org/journal/apchd5

Doping-Induced Self-Absorption in Light-Emitting Electrochemical Cells

Nikolai Kaihovirta, Amir Asadpoordarvish, Andreas Sandström, and Ludvig Edman*

The Organic Photonics and Electronics Group, Department of Physics, Umeå University, SE-901 87 Umeå, Sweden

ABSTRACT: We report on the quantitative effects of doping-induced self-absorption in light-emitting electrochemical cells (LECs) as a function of active material (AM) thickness and doping concentration. For state-of-the-art polymer LECs with optimized doping concentration and comprising Super Yellow as the electroluminescent (EL) polymer and poly(ethylene oxide)-KCF_3SO_3 as the electrolyte, we find that the self-absorption loss at the EL peak wavelength is ∼10% for a 100 nm thin AM and >70% for a 1 μm thick AM. This implies that the utilization of micrometer-thick AMs fit for fault-tolerant large-scale fabrication can be concomitant with a notable penalty in device performance, and that spatial variations in AM thickness will be manifested in a corresponding spatial light-intensity variation. Moreover, we find that inclusion of a poly(ethylene oxide)-KCF_3SO_3 electrolyte can inhibit the out-coupling of light and suggest that the culprit is light scattering from dispersed crystalline-electrolyte domains. Finally, we demonstrate evidence for that the selected initial salt concentration in an LEC device dictates the maximum doping concentration that can be attained at steady-state operation.

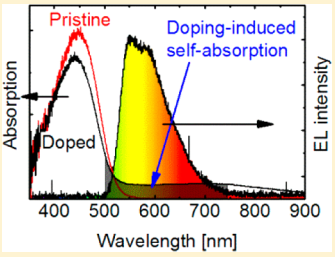

KEYWORDS: *light-emitting device, organic electronics, electroluminescence, electrochemical doping, cyclic voltammetry, conjugated polymer*

The light-emitting electrochemical cell (LEC) is an emerging emissive technology that operates under the novel realm of in situ electrochemical doping.[1−7] The active material in an LEC comprises a blend of a luminescent conjugated compound and mobile ions, which is sandwiched between two charge-injecting electrodes.[8,9] The ions redistribute when a voltage is applied between the electrodes so that electrochemistry can be initiated at the two electrode interfaces, being electrochemical p-type doping at the positive anode and n-type doping at the negative cathode.[10−12] With time, the conductive doped regions grow in size to eventually make contact under the formation of a light-emitting p−n junction in the bulk of the active material.[13−18] This intriguing electrochemical doping process brings a number of important advantages unique to the LEC technology, notably the opportunity for the employment of air-stable and solution-processable materials for both electrodes and the utilization of thick and uneven active materials.[19−23] These characteristic LEC features in turn pave the way for a fault-tolerant, scalable, and low-cost fabrication of large-area emissive sheets under ambient air conditions, using, for example, roll-to-roll (R2R) compatible coating and printing technologies.[24,25]

However, it has recently been realized that the electrochemical operation and in situ doping process can bring some drawbacks, notably electrochemical side reactions at the electrode interfaces[26,27] and doping-induced exciton quenching and chemical side-reaction at, or next to, the location of the p−n junction.[28−30] Fortunately, it has also been demonstrated that these drawbacks can be effectively alleviated via a rational device design, including the employment of electrochemically stable electrode materials,[26] the development of an appropriate drive scheme,[28,31,32] and the implementation of an optimized salt-to-conjugated-compound ratio.[28] The merit of these procedures is clearly manifested in recent demonstrations of LEC devices with distinctly improved lifetimes and efficiencies.[28,32−34]

In this article, we investigate an often overlooked loss mechanism specific to LEC devices, namely, doping-induced self-absorption. It originates in the well-established fact that doping causes significant changes of the optical properties of conjugated compounds, specifically a red-shift of the absorption, with the consequence that the (here, undesired) emission-absorption overlap of the device increases.[35−37] By utilizing a combination of cyclic voltammetry (CV) and absorption spectroscopy (see Figure 1a), we are able to establish the correlation between the doping concentration and the absorption coefficient for the conjugated polymer Super Yellow. By then measuring the in situ absorption changes in the active material of Super Yellow-based LECs during operation, we can determine the temporal evolution of the doping concentration and, for example, establish that the maximum doping concentration, as expected for a functional device,[38,39] is dictated by the initial ion concentration. We are also able to establish a relationship between the self-absorption loss and the active material thickness for a number of different LEC devices, comprising different levels of doping. Specifically, we find that for a doping-optimized ITO/{Super Yellow+PEO+KCF_3SO_3}/Al device (for chemical structure of the compounds in the active layer and the device structure, see Figure 1b and c, respectively), the self-absorption loss at the Super Yellow

Received: September 20, 2013
Published: February 3, 2014

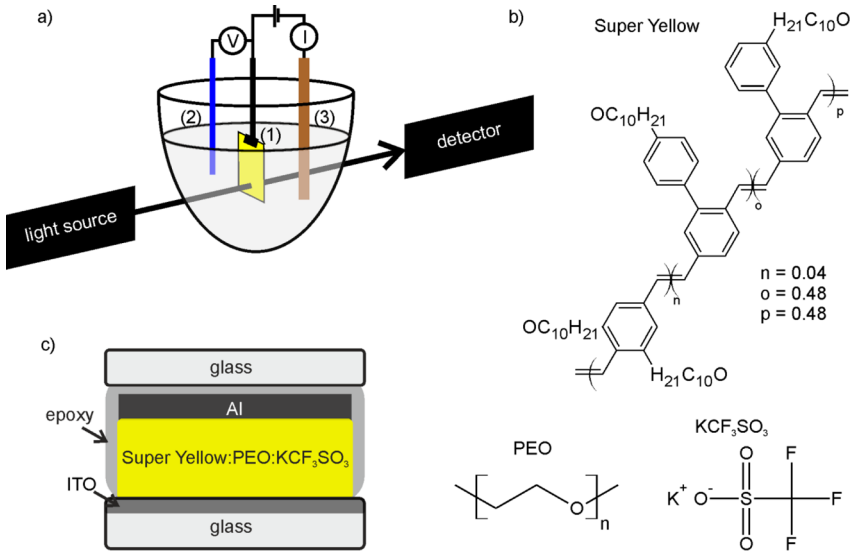

Figure 1. (a) Combined CV-absorption spectroscopy setup: The numbers depict (1) the working electrode, (2) the reference electrode, and (3) the counter electrode; (b) Chemical structure of the constituents in the LEC active material; (c) LEC device structure.

electroluminescence (EL) peak is ~10% for a 100 nm thick active material and a staggering >70% for a 1 μm thick active material. Importantly, these findings imply that the employment of thick active material films fit for, for example, R2R-coating can be concomitant with a severe penalty in device efficiency and also result in an uneven light emission.

RESULTS AND DISCUSSION

Figure 2a presents CV scans recorded with the wprking electrode being bare ITO (black line) and Super Yellow-on-

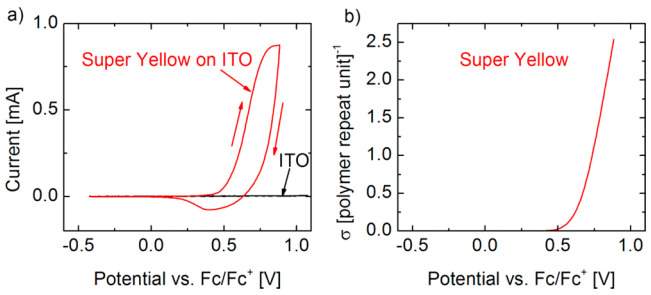

Figure 2. (a) Back-and-forth CV traces using Super Yellow-on-ITO (red line) and bare ITO (black line) as the working electrode. The scan rate was 25 mV/s. (b) Super Yellow doping concentration as a function of CV potential.

ITO (red line), respectively. The absence of current peaks in the bare ITO reference trace demonstrates that all other constituents than Super Yellow (i.e., electrolyte and ITO), as desired, are electrochemically inert in the probed CV potential range. The onset potential for p-type doping of Super Yellow is +0.5 V versus Fc/Fc$^+$, and this value as well as the qualitative shape of the Super Yellow CV trace are in good agreement with an earlier report.[40]

It is possible to calculate the doping level of an electroactive compound as a function of CV potential by integrating the current in the forward CV scan and by assuming that this charge ($Q = \int I dt$) is consumed solely by electrochemical doping. The doping concentration (σ) is then given by the following equation:

$$\sigma = (Q \times M_{EC})/(V_{EC} \times \rho_{EC} \times N_A \times e) \quad (1)$$

where M_{EC} is the molar mass of the electroactive compound, V_{EC} is its volume, ρ_{EC} is its density, N_A is Avogadro's constant, and e is the elementary charge. By including our specific values of M_{EC} = 350 g/mol (the molar mass of the average Super Yellow repeat unit), $V_{EC} = 1.17 \times 10^{-5}$ cm^3, and ρ_{EC} = 1 g/cm^3 (the estimated density of the Super Yellow film), we are able to calculate the doping concentration of Super Yellow as a function of CV potential, as shown in Figure 2b. The doping concentration exhibits a superlinear increase with CV potential; a trend that is in good agreement with earlier studies on the conjugated polymers poly(2,5-diethoxy-*p*-phenylene vinylene) and poly(1,4-naphtalene vinylene) by Onoda et al.[41,42] We further note that the doping concentration at the maximum current point in the CV measurement (+0.9 V vs Fc/Fc$^+$) is very high at 2.5 dopants per Super Yellow repeat unit.

The absorption of the Super Yellow film was measured in situ at different times during the CV measurement using the setup shown in Figure 1a. By utilizing the Beer–Lambert law

$$I/I_0 = \exp(-\alpha \times d) \quad (2)$$

where I and I_0 are the measured light intensity with and without the Super Yellow film included in the beam path, respectively, and d is the Super Yellow film thickness (=120 nm); it is possible to obtain the absorption coefficient (α) of Super Yellow at different CV potentials. Figure 3a presents α_{SY} as a function of wavelength (λ) for a pristine Super Yellow film (black solid squares) and a p-type doped Super Yellow film (red open circles); the latter data were recorded at +0.5 V versus Fc/Fc$^+$. Anticipated consequences of doping Super Yellow are a decrease (bleaching) of the π–π^* absorption band with a peak at 450 nm and an emergence of doping-induced (polaron) absorption bands at longer wavelengths,[36] as are indeed observed in Figure 3a.

Figure 3a also includes the EL spectrum of a Super Yellow-based LEC with a 70 nm thin active material (blue solid triangles), and it is notable that the EL exhibits a strong overlap with the absorption of p-type doped Super Yellow but much less so with pristine Super Yellow. Sandwich-cell LECs are commonly constructed so that the positive anode is the

dx.doi.org/10.1021/ph400050t | ACS Photonics 2014, 1, 182–189

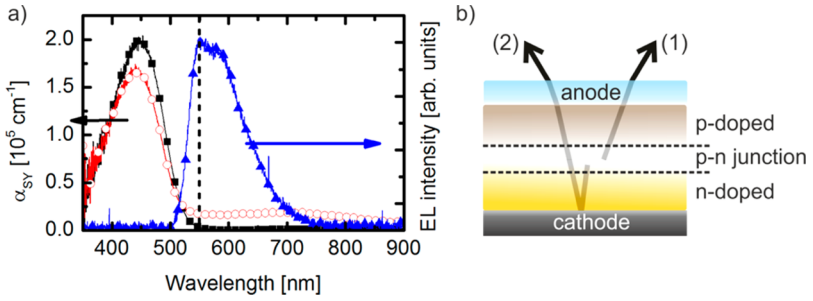

Figure 3. Absorption spectra of a pristine Super Yellow film (black solid squares) and a doped Super Yellow film (red open circles), as measured in the CV setup. EL spectrum from a thin-active material LEC (blue solid triangles). (b) Schematic representation of two scenarios for the out-coupling of light from an LEC, with the p−n junction doping structure in place: (1) depicts light out-coupled directly via passage through the p-type doped region and the transparent anode and (2) depicts light that is first reflected off the reflective cathode and, thereby, in addition, is passing through the n-type doped region twice.

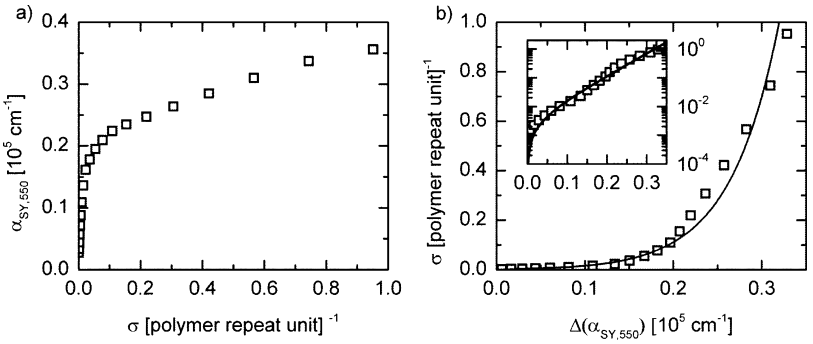

Figure 4. (a) Absorption coefficient of Super Yellow at λ = 550 nm as a function of doping concentration. (b) Doping concentration of Super Yellow as a function of the change in the absorption coefficient. The solid line represents a fit to the measured data. The inset shows the same plot in a semilogarithmic scale.

transparent electrode, which implies that the light always must pass through a p-type-doped region formed at the anode before exiting the device, regardless of whether the light is initially directed toward the transparent anode or reflected off the metallic cathode, as shown as scenario (1) and (2), respectively, in Figure 3b. Moreover, we find significantly smaller changes in the optical absorption of the Super Yellow film during n-type doping, specifically a much smaller overlap between the absorption of n-type-doped Super Yellow and the Super Yellow EL. This asymmetry in the optical response to p-type doping versus n-type doping corresponds to the findings in an earlier study on another electroluminescent poly(para-phenylene vinylene) polymer, namely, poly[2-methoxy-5-(2-ethylhexyloxy)-1,4-phenylenevinylene] (MEH-PPV).[43] Importantly, these observations suggest that p-type doping-induced self-absorption can be a prominent and performance-limiting feature during the operation of LEC devices, particularly for devices featuring a thick active material as this self-absorption will increase with the thickness of the active material, and it is something we will investigate further below.

Figure 4a presents the combined results of the preceding CV and optical absorption measurements as the Super Yellow absorption coefficient at λ = 550 nm ($\alpha_{SY,550}$) as a function of Super Yellow doping concentration (σ). We selected to focus on $\alpha_{SY,550}$, since the peak EL wavelength of the Super Yellow-based LEC is positioned at λ = 550 nm (see dotted line in Figure 3a). It is noteworthy that $\alpha_{SY,550}$ is found to be highly sensitive to σ at low doping concentrations (<0.1 dopants per Super Yellow repeat unit) but less so at higher values. Indeed, during the forward CV sweep, the Super Yellow film is observed to rapidly turn from yellow color into dark green promptly above the onset voltage for p-type doping, while at higher voltages and doping concentrations, the color change is less significant. A similar qualitative change in the optical absorption of other conjugated polymers can be deduced from the work by Onoda et al.[41,42]

A closer inspection of Figures 3a and 4a reveals that the pristine and undoped Super Yellow polymer exhibits a minor absorption (0.03×10^5 cm^{-1}) at λ = 550 nm. In order to attain information on the *changes* in absorption induced exclusively by doping, we have in Figure 4b subtracted this baseline value for the presentation of σ as a function of the change in Super Yellow absorption at λ = 550 nm, $\Delta(\alpha_{SY,550})$. We were able to attain a good fit to our experimental σ versus $\Delta(\alpha_{SY,550})$ data with the following function (included as the solid line in Figure 4b):

$$\sigma = 0.003 \times [\exp(\Delta(\alpha_{SY,550})/5500) - 1] \quad (3)$$

We now shift our attention to the doping-induced self-absorption in LEC devices and its influence on device performance. We have previously shown that the maximum attainable average doping concentration in an LEC device at steady-state is dictated by the selected initial ion concentration in the active material, based on the insight that each ion is effectively neutralized ("consumed") by one dopant during the in situ doping process.[28,38] By rearranging the terms in the equation derived in ref 28, we are able to attain the dependence of the maximum average steady-state doping concentration (x_{doping}) on the mass ratio between the salt and the electroactive compound (m_{salt}/m_{EC}), the thickness of the active material

dx.doi.org/10.1021/ph400050t | ACS Photonics 2014, 1, 182−189

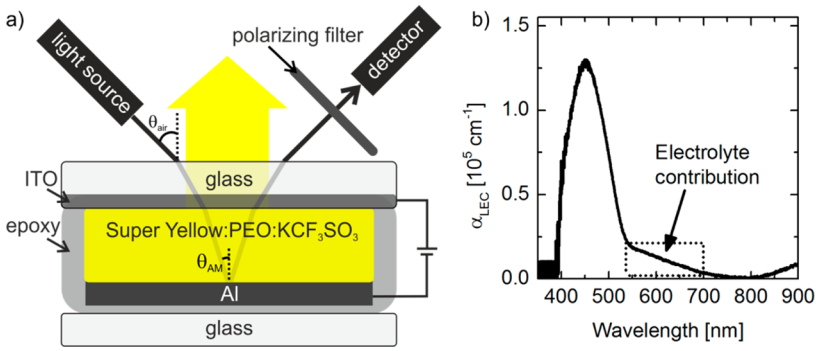

Figure 5. (a) Schematic of the experimental setup for the in situ measurement of absorption in operating LEC devices. (b) Absorption spectrum of the pristine active material in an LEC device. The dotted rectangle indicates the contribution assigned to the electrolyte component in the active material.

(d_{AM}), the molar mass of the salt (M_{salt}), and the estimated thickness of the p−n junction (d_{pn}):

$$x_{doping} = (2 \times m_{salt} \times d_{AM} \times M_{EC}) / (m_{EC} \times (d_{AM} - d_{pn}) \times M_{salt}) \quad (4)$$

By including selected and measured values of $m_{salt}/m_{EC} = 0.1$, $d_{AM} = 70$ nm, $M_{EC} = 350$ g/mol (the molar mass of the average Super Yellow repeat unit), $M_{salt} = 188$ g/mol, and an estimated value of $d_{pn} \sim 10$ nm, we find that the maximum average steady-state doping concentration is $x_{doping} = 0.4$ dopants per Super Yellow repeat unit for our herein studied LEC devices. We note that this value is relatively independent of the estimated value for d_{pn} within a reasonable d_{pn} range. We also emphasize that we have selected to employ a higher value for the electrolyte concentration than required for optimum device performance,[28,40] with the motivation being that it will allow for a higher doping level so that the effects of the doping-induced self-absorption will be corroborated; we will however include a discussion on the effects of self-absorption for performance-optimized devices at the end of this article.

We measured the in situ absorption of the active material in our LEC devices using the setup presented in Figure 5a. In order to translate the measured I and I_0 values to an absorption coefficient, we needed to know the effective thickness, d, to include in eq 2, which is the distance the probing beam has traversed during the absorption measurement. By employing Snell's law, $n_1 \sin\theta_1 = n_2 \sin\theta_2$, setting $n_{air} = 1$, $n_{AM} = 1.9$,[44] and measuring $\theta_{air} = 45°$, we find that $\theta_{AM} = 22°$. With a measured active material thickness of 70 nm for our devices, and taking into account that the probing beam is reflected off the Al cathode before entering the detector and, thus, passing through the active material twice during the measurement, we find that the effective thickness to be included in eq 2 is $d = 151$ nm.

With this information at hand, we were able to attain the absorption coefficient for a pristine {Super Yellow/PEO/KCF_3SO_3} active material film as a function of wavelength as the black line in Figure 5b. We find that the peak absorption coefficient at $\lambda = 450$ nm for the pristine {Super Yellow/PEO/KCF_3SO_3} active LEC material is $\alpha_{LEC,450} = 1.3 \times 10^5$ cm^{-1}, which is 36% lower than for the pure Super Yellow film (see Figure 3a). This is in good agreement with what could be anticipated, based on that the active material film is "diluted" by 33% electrolyte by mass. Importantly, we further find that the absorption spectrum of the pristine active material features a broad shoulder with significant magnitude at 550−700 nm (as indicated by the dotted rectangle in Figure 5b), which is absent in the pure Super Yellow absorption spectrum. The finding of a shoulder is supported by an independent measurement on the same active material at normal incidence. We assign this shoulder to the existence of the electrolyte in the active material; more specifically, we propose that it stems from light scattering by crystalline PEO or PEO:KCF_3SO_3 domains, which can be prominent features at room temperature.[45,46] The value for the effective absorption coefficient of the pristine active material at $\lambda = 550$ nm is $\alpha_{LEC,550} = 0.19 \times 10^5$ cm^{-1}, and it stems primarily from the dispersed electrolyte component but also from a minor absorption of pristine Super Yellow (see Figure 4a and accompanying discussion). By subtracting the contribution of the latter, the absorption coefficient of the electrolyte in our LEC devices is found to amount to $\alpha_{LEC\text{-}Elec,550} = 0.16 \times 10^5$ cm^{-1}.

At this point, it is relevant to remind ourselves that the active material of an LEC device comprises three different regions during light-emission: a p-type doped region next to the anode, an n-type doped region next to the cathode, and a p−n junction sandwiched in between the two doped regions (see Figure 3b). In order to delineate the effects from these different regions, we choose to focus on the absorption at $\lambda = 550$ nm, since our CV-absorption measurements disclosed that it is primarily p-type doped (and not pristine or n-type doped) Super Yellow that absorbs light at this wavelength. To estimate the thickness of the p-type doped region, we assume: (i) a symmetric doping profile and (ii) that the p−n junction is 10 nm thick. With these assumptions in place, we find that the thickness of the p-type doped region in the herein studied LEC devices is 30 nm. By using Snell's law as detailed above and taking into account the double pass of the probing beam through the active material, we find that the value for the effective thickness to be plugged into eq 2 is $d = 65$ nm. Moreover, in order to separate out the effects of the electrolyte-induced background in LEC devices (see Figure 5b and accompanying discussion), we have selected to focus on the change in the absorption coefficient at $\lambda = 550$ nm with respect to the pristine active material, that is, $\Delta(\alpha_{LEC,550})$.

Figure 6 presents the measured $\Delta(\alpha_{LEC,550})$ as a function of time during LEC operation in the form of solid black squares. We find that the changes in absorption of the active material in the LEC are most prominent during the early stages of device operation. By approximating the changes in absorption in the LEC film at $\lambda = 550$ nm with that of the electrolyte-free Super Yellow film, and thereafter, importing these values into the herein derived translation table (see Figure 4b), we are able to

dx.doi.org/10.1021/ph400050t | ACS Photonics 2014, 1, 182−189

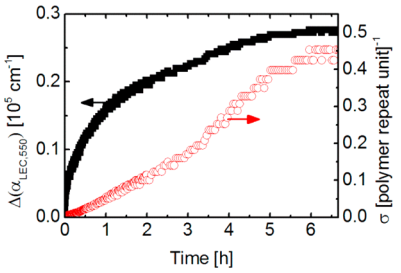

Figure 6. Measured change in the absorption coefficient of the LEC active material at λ = 550 nm as a function of time (solid black squares). The temporal evolution of the Super Yellow p-type doping concentration in an operating LEC device (open red circles).

obtain information on the temporal development of the Super Yellow doping concentration in an LEC device. More specifically, by setting $\Delta(\alpha_{SY,550}) = \Delta(\alpha_{LEC,550})$ and importing these discrete data into the fit function disclosed in eq 3, we could track the evolution of the average p-type doping concentration as a function of time, as presented by the open red circles in Figure 6.

We observe a superlinear increase of the average p-type doping concentration with time during the first few hours of operation and note that this observation is in agreement with that the speed of the p-type doping front in planar surface cells, which provides an estimate on the p-type doping concentration, has been found to also increase with time during the early stages of device operation.[47] We further note that the p-type doping concentration saturates at a value of 0.4−0.5 dopants per Super Yellow repeat unit after 6 h of operation, which is close to our calculated value for the maximum steady-state doping concentration in this particular LEC device, x_{doping} = 0.4 dopants per Super Yellow repeat unit, as dictated by eq 4. We wish to point out that the performance of this device is inferior to that of optimized devices with a lower electrolyte content[28,40] and that we as expected find that the device performance begins to deteriorate during the early stages of operation; specifically, we find that the current density levels off already at ∼0.1 h and that the luminance and the power conversion efficacy begins to decrease at t > 0.5 h. We suggest that the early degradation in performance can be attributed to the attainment of a too-high doping level (x_{doping} > 0.1[28]) at this point in time, which will cause doping-induced and undesired exciton-quenching and side reactions, as discussed in detail in refs 28 and 29 but also, notably, significant doping-induced self-absorption.

To better illustrate the consequences of doping-induced self-absorption for LECs with different doping concentration and thickness, we have selected to present data for a number of relevant scenarios in Figure 7. We have assumed that the light is directed at normal incidence toward one of the two electrode interfaces and thereafter coupled out of the device directly (i.e., the light is only passing through the p-type region once); the presented data in Figure 7 thus represent a lower limit on the effects of self-absorption. Moreover, for clarity we have only presented data for the self-absorption at λ = 550 nm.

Figures 7a and b present the transmittance (I/I_0) of the p-type doping region as a function of the p-type doping layer thickness, as calculated using eq 2. In scenario (i), the transmittance is derived from a doping concentration of 0.4 dopants per Super Yellow repeat unit ($\alpha_{550} = 0.28 \times 10^5$ cm^{-1}; see Figure 4a); whereas in scenario (ii), the transmittance is derived for a lower doping concentration of 0.1 dopants per Super Yellow repeat unit ($\alpha_{550} = 0.22 \times 10^5$ cm^{-1}; see Figure 4a). In Figure 7b, we consider the total transmittance-blocking effect of the p-type doped region, by also including the loss contribution from the dispersed PEO-based electrolyte. In scenario (iii), we consider a doping concentration of 0.4 dopants per Super Yellow repeat unit, and the existence of a scattering electrolyte component, i.e. $\alpha_{550} = (0.28 + 0.16) \times 10^5$ cm^{-1} = 0.44×10^5 cm^{-1}. Scenario (iv) then depicts the transmittance that will occur with a doping concentration of 0.1 dopants per Super Yellow repeat unit and the existence of a scattering electrolyte. Note that the contribution by the electrolyte has been divided by four in this latter scenario, as a lower maximum doping concentration by a factor of 4 is concomitant with a decreased electrolyte (strictly the salt) mass ratio by the same factor; see eq 4. Thus, for scenario (iv), $\alpha_{550} = (0.22 + 0.25 \times 0.16) \times 10^5$ cm^{-1} = 0.26×10^5 cm^{-1}.

If we again assume that the p−n junction is 10 nm thick and symmetrically placed in the middle of the active material and neglect the effects of self-absorption of the n-type region, we can replot the transmittance data as the self-absorption (= 1 − transmittance) as a function of the total active material thickness. These data are displayed in Figure 7c. We note that the self-absorption loss at steady-state operation for an LEC comprising a thin active material film of 100 nm thickness is 11% at λ = 550 nm for an optimized low doping concentration (0.1 dopants per Super Yellow repeat unit)

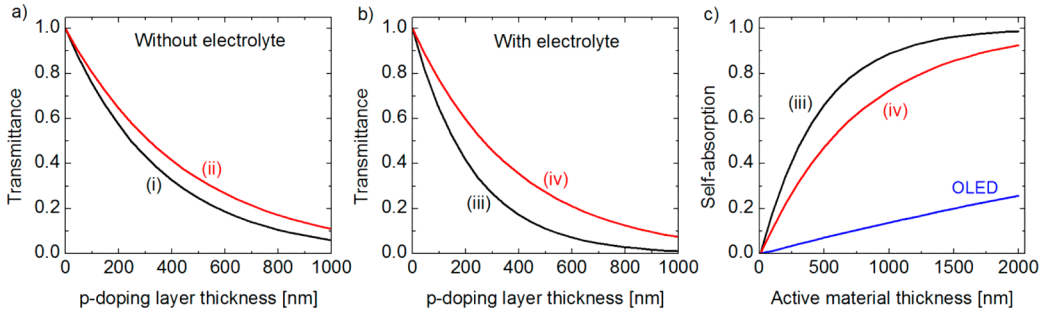

Figure 7. (a) Transmittance at λ = 550 nm as a function of p-type doping layer thickness for (i) 0.4 dopants per Super Yellow repeat unit (black line) and (ii) 0.1 dopants per Super Yellow repeat unit (red line). (b) Transmittance at λ = 550 nm for (iii) the high (black line) and (iv) the low (red line) doping concentration, taking into account also the loss effects from the electrolyte. (c) LEC self-absorption at λ = 550 nm as a function of active material thickness for (iii) the high (black line) and (iv) the low (red line) doping concentration. The blue line depicts the self-absorption loss in a doping- and electrolyte-free Super Yellow-based OLED.

dx.doi.org/10.1021/ph400050t | ACS Photonics 2014, 1, 182−189

and 18% at a high doping concentration (0.4 dopants per Super Yellow repeat unit). However, the situation turns much more problematic for LECs comprising active material films of larger thickness. A 500 nm thick LEC film features a self-absorption loss of 47% at the low doping concentration and 66% at the high doping concentration, whereas micrometer-thick LEC films exhibit self-absorption losses in excess of 70% also for an optimized low doping concentration. These results imply that significant self-absorption losses are a common feature in thick LEC films fit for fault-tolerant and scalable R2R fabrication and that it is not realistic to anticipate peak efficiencies from such thick-film devices, which are using the same conjugated compound for both charge transport and light emission.[48]

In Figure 7c, we have for comparison also included the self-absorption data for a Super Yellow-based OLED, as calculated using the absorption coefficient for pristine Super Yellow ($\alpha_{SY,550} = 0.03 \times 10^5$ cm^{-1}; see Figure 3a). As expected, we find that the effects of self-absorption is comparatively minor for this polymer OLED, and note that the self-absorption for such a polymer OLED with a practical active material thickness of 100 nm is a mere 1% at $\lambda = 550$ nm. Thus, it again becomes clear that the OLED and LEC are two distinctly different device technologies, each with its own specific set of pros and cons.

Importantly, the presented results suggest that the efficiency of LEC devices with thick active layers, that is, the typical outcome of a scalable and low-cost R2R fabrication process, is going to be subpar unless appropriate measures are employed. Such procedures could involve the employment of host−guest systems to decrease the overlap between the emission of the guest and the absorption of a doped host or the utilization of a transparent cathode, so that half of the light generated in the p−n junction only passes through a weakly absorbing n-type doped regions before exiting the device; see Figure 3b for schematic. Moreover, it is important to point out that the performance of thin-film light-emitting devices, such as LECs and OLEDs, also can be heavily influenced by other factors, such as microcavity effects and optical waveguiding, as discussed, for example, in refs 22 and 49. We are currently working on an expanded study on LEC devices that incorporates these effects as well and hope to be able to present these results in a future publication.

Finally, we wish to point out that our findings predict that undesired variations in the EL intensity and color over the device area can be a prominent feature from LEC devices comprising thick films with a spatial variation in thickness. First, as the thinner regions will exhibit a smaller self-absorption loss, they will feature a corresponding higher EL intensity than the thicker regions. Second, if the self-absorption exhibits a wavelength-dependency, one can compare the doped region with a filter, which allows certain wavelengths to pass more easily. Two manifestations of this latter phenomenon are (i) that thicker active material films will feature a different EL color (and lower intensity) than thinner films and (ii) that uneven films will display color variations over the device area.

SUMMARY

We demonstrate that doping-induced self-absorption can be an undesired prominent feature in conventional LECs. Specifically, we show that a subpar device efficiency results from the employment of thick active materials, and that a spatial variation in EL intensity is anticipated from devices featuring uneven thickness for the active material. We specifically investigate a Super Yellow-based LEC and show that the loss due to self-absorption can amount to 66% for a 500 nm thick active material at steady-state operation. Moreover, we also establish the relationship between the absorption and doping concentration for Super Yellow and demonstrate that the maximum doping concentration that can be attained in an LEC device is dictated by the initial salt concentration.

METHODS

For the preparation of CV experiments, the following procedure was used. A glass substrate partially covered with indium tin oxide (ITO; Thin Film Devices, U.S.A.) was washed with acetone and isopropanol and thereafter dried in an oven at $T = 120$ °C for $t > 3$ h. The electroluminescent phenyl-substituted poly(*para*-phenylene vinylene) copolymer ("Super Yellow", Merck)[50] was dissolved in cyclohexanone and thereafter spin-coated onto the cleaned ITO-coated glass substrate; for the chemical structure of Super Yellow, see Figure 1b. The Super Yellow film was dried on a hot plate at $T = 70$ °C for $t > 12$ h, and the thickness of the dry film was 120 nm, as measured with a stylus profilometer (Dektak XT, Bruker). The electrolyte comprised the salt KCF_3SO_3 (dried under vacuum at $T = 200$ °C, Aldrich) dissolved in acetonitrile (anhydrous, Aldrich) in a molar concentration of 0.04 M. Bare ITO or Super Yellow-on-ITO was used as the working electrode (WE), and the active area of the WE was 1.50 × 0.65 cm^2. A quartz glass crucible was filled with electrolyte solution and enclosed with a PTFE lid. The WE (1), a platinum-rod counter electrode (3), and a silver-rod quasi-reference electrode (2) were immersed into the electrolyte solution, as depicted in Figure 1a. All sample fabrication was done in a N_2-filled glovebox ($[O_2]$, $[H_2O] < 1$ ppm). The CV measurements were driven by an Autolab PGSTAT302 potentiostat and controlled by the GPES (EcoChemie) software. The voltage step and scanning speed were 10 mV/step and 25 mV/s, respectively. At the end of each CV measurement, a small amount of ferrocene (Fluka) was added to the electrolyte solution, and a calibration scan was performed in order to determine the potential of the ferrocene/ferrocenium ion (Fc/Fc^+) redox couple, which established the reference potential.

The absorption spectra of Super Yellow were recorded in situ during the CV measurements, as illustrated schematically in Figure 1a. The light source was a tungsten halogen lamp (HL-2000-HP-RS-232, Ocean Optics), and the probing light was coupled onto the WE via an optical fiber (Ocean Optics). The detection was carried out by coupling the transmitted light into a second optical fiber, which carried the transmitted light to the detector being a high-resolution spectrometer (HR 4000, Ocean Optics). The integration time for one scan was 4 ms, and 100 such scans were averaged for each presented spectrum. The recorded data were analyzed using the SpectraSuite software (Ocean Optics).

The device structure for the LEC sandwich cells is shown in Figure 1c, and they were prepared as follows. Precleaned ITO-coated glass substrates were used as the anode. The active material comprised a blend of Super Yellow, the ion-dissolving and ion-transporting polymer poly(ethylene oxide) (PEO, $M_W = 5 \times 10^6$, Aldrich), and the salt KCF_3SO_3 (Aldrich), with chemical structures depicted in Figure 1b. The PEO and KCF_3SO_3 were dried under vacuum at $T = 50$ °C and $T = 200$ °C, respectively. The active-material constituents were separately dissolved in cyclohexanone (Aldrich) in a concentration of 7 g/L (Super Yellow) and 10 g/L (PEO and

dx.doi.org/10.1021/ph400050t | ACS Photonics 2014, 1, 182−189

KCF_3SO_3), and these master solutions were thereafter mixed together in a mass ratio of {Super Yellow/PEO/KCF_3SO_3} = (1:0.4:0.1). The blend solution was spin-coated onto the ITO anode at 2000 rpm for 60 s and, thereafter, dried on a hot plate at T = 50 °C for t > 16 h. The thickness of the dry active material was 70 nm, as measured with the stylus profilometer. On top of the active material, an Al cathode was deposited by thermal evaporation at $p < 2 \times 10^{-6}$ mbar through a shadow mask. The light-emitting area, as defined by the size of the Al cathode, was 0.80 × 0.80 cm^2. The LEC devices were encapsulated by attaching a glass plate onto the Al-side of the device using a UV-curable single-component epoxy adhesive (Ossila). More details on the encapsulation procedure have been reported elsewhere.[51] All LEC device preparation took place in two interconnected N_2-filled glove boxes ([O_2], [H_2O] < 1 ppm).

The LEC devices were driven at constant voltage V = 4 V by an Agilent E3647A DC power supply, with ITO biased as the positive anode. The absorption spectra of the active material were recorded in situ during LEC operation by collecting the remaining probing light reflected from the Al cathode, as illustrated in Figure 5a. The absorption spectroscopy setup was identical to that described above, with the exceptions being that the light source and detector were placed at an angle of 45° with respect to the LEC surface, and that a polarizing filter was placed in front of the detector. The EL spectrum was recorded normal to the LEC surface using a high-resolution spectrometer (HR 4000, Ocean Optics). The encapsulated LECs were operated and probed under ambient air.

AUTHOR INFORMATION

Corresponding Author

*Phone: +46-90-7865732. Fax: +46-90-7866672. E-mail: ludvig.edman@physics.umu.se.

Notes

The authors declare no competing financial interest.

ACKNOWLEDGMENTS

The authors acknowledge Vetenskapsrådet, Energimyndigheten, Kempestiftelserna, Carl Trygger's foundation and Umeå University for financial support. L.E. is a "Royal Swedish Academy of Sciences Research Fellow" supported by a grant from the Knut and Alice Wallenberg Foundation.

REFERENCES

(1) Pei, Q. B.; Yang, Y.; Yu, G.; Zhang, C.; Heeger, A. J. Polymer light-emitting electrochemical cells: In situ formation of a light-emitting p−n junction. *J. Am. Chem. Soc.* **1996**, *118*, 3922−3929.

(2) Pei, Q. B.; Yu, G.; Zhang, C.; Yang, Y.; Heeger, A. J. Polymer light-emitting electrochemical cells. *Science* **1995**, *269*, 1086−1088.

(3) Matyba, P.; Maturova, K.; Kemerink, M.; Robinson, N. D.; Edman, L. The dynamic organic p−n junction. *Nat. Mater.* **2009**, *8*, 672−676.

(4) van Reenen, S.; Matyba, P.; Dzwilewski, A.; Janssen, R. A. J.; Edman, L.; Kemerink, M. A unifying model for the operation of light-emitting electrochemical cells. *J. Am. Chem. Soc.* **2010**, *132*, 13776−13781.

(5) Meier, S. B.; van Reenen, S.; Lefevre, B.; Hartmann, D.; Bolink, H. J.; Winnacker, A.; Sarfert, W.; Kemerink, M. Dynamic doping in planar ionic transition metal complex-based light-emitting electrochemical cells. *Adv. Funct. Mater.* **2013**, *23*, 3531−3538.

(6) Leger, J. M. Organic electronics: The ions have it. *Adv. Mater.* **2008**, *20*, 837−841.

(7) van Reenen, S.; Kersten, S. P.; Wouters, S. H. W.; Cox, M.; Janssen, P.; Koopmans, B.; Bobbert, P. A.; Kemerink, M. Large magnetic field effects in electrochemically doped organic light-emitting diodes. *Phys. Rev. B* **2013**, *88*, 125203.

(8) Hernandez-Sosa, G.; Eckstein, R.; Tekoglu, S.; Becker, T.; Mathies, F.; Lemmer, U.; Mechau, N. The role of the polymer solid electrolyte molecular weight in light-emitting electrochemical cells. *Org. Electron.* **2013**, *14*, 2223−2227.

(9) Zysman-Colman, E.; Slinker, J. D.; Parker, J. B.; Malliaras, G. G.; Bernhard, S. Improved turn-on times of light-emitting electrochemical cells. *Chem. Mater.* **2008**, *20*, 388−396.

(10) He, L.; Duan, L.; Qiao, J.; Zhang, D. Q.; Dong, G. F.; Wang, L. D.; Qiu, Y. Electrophosphorescent devices based on cationic iridium complexes: The effect of fluorinating the pendant phenyl ring of the ancillary ligand on the device performances. *Synth. Met.* **2013**, *166*, 52−56.

(11) Toshner, S. B.; Zhu, Z. H.; Kosilkin, I. V.; Leger, J. M. Characterization of ion profiles in light-emitting electrochemical cells by secondary ion mass spectrometry. *ACS Appl. Mater. Interfaces* **2012**, *4*, 1149−1153.

(12) Georgiadou, D. G.; Palilis, L. C.; Vasilopoulou, M.; Pistolis, G.; Dimotikali, D.; Argitis, P. Influence of the anion on the optoelectronic characteristics of triphenylsulfonium salts modified polymer light emitting devices. *Synth. Met.* **2013**, *181*, 37−44.

(13) Gao, J.; Dane, J. Planar polymer light-emitting electrochemical cells with extremely large interelectrode spacing. *Appl. Phys. Lett.* **2003**, *83*, 3027−3029.

(14) Gao, J.; Dane, J. Visualization of electrochemical doping and light-emitting junction formation in conjugated polymer films. *Appl. Phys. Lett.* **2004**, *84*, 2778−2780.

(15) Wang, T. W.; Su, H. C. Extracting evolution of recombination zone position in sandwiched solid-state light-emitting electrochemical cells by employing microcavity effect. *Org. Electron.* **2013**, *14*, 2269−2277.

(16) Liu, J.; Engquist, I.; Crispin, X.; Berggren, M. Spatial Control of p−n junction in an organic light-emitting electrochemical transistor. *J. Am. Chem. Soc.* **2012**, *134*, 901−904.

(17) Liu, J.; Engquist, I.; Berggren, M. Double-gate light-emitting electrochemical transistor: confining the organic p−n junction. *J. Am. Chem. Soc.* **2013**, *135*, 12224−12227.

(18) Jhang, Y.-P.; Chen, H.-F.; Wu, H.-B.; Yeh, Y.-S.; Su, H.-C.; Wong, K.-T. Improving device efficiencies of solid-state white light-emitting electrochemical cells by adjusting the emissive-layer thickness. *Org. Electron.* **2013**, *14*, 2424−2430.

(19) Matyba, P.; Yamaguchi, H.; Chhowalla, M.; Robinson, N. D.; Edman, L. Flexible and metal-free light-emitting electrochemical cells based on graphene and PEDOT-PSS as the electrode materials. *ACS Nano* **2011**, *5*, 574−580.

(20) Yu, Z. B.; Hu, L. B.; Liu, Z. T.; Sun, M. L.; Wang, M. L.; Gruner, G.; Pei, Q. B. Fully bendable polymer light emitting devices with carbon nanotubes as cathode and anode. *Appl. Phys. Lett.* **2009**, *95*, 203304.

(21) Matyba, P.; Yamaguchi, H.; Eda, G.; Chhowalla, M.; Edman, L.; Robinson, N. D. Graphene and mobile ions: The key to all-plastic, solution-processed light-emitting devices. *ACS Nano* **2010**, *4*, 637−642.

(22) Li, X. Y.; Gao, J.; Liu, G. J. Thickness dependent device characteristics of sandwich polymer light-emitting electrochemical cell. *Org. Electron.* **2013**, *14*, 1441−1446.

(23) Inganas, O. Hybrid electronics and electrochemistry with conjugated polymers. *Chem. Soc. Rev.* **2010**, *39*, 2633−2642.

(24) Sandström, A.; Dam, H. F.; Krebs, F. C.; Edman, L. Ambient fabrication of flexible and large-area organic light-emitting devices using slot-die coating. *Nat. Commun.* **2012**, *3*, 1002.

(25) Liang, J. J.; Li, L.; Niu, X. F.; Yu, Z. B.; Pei, Q. B. Fully solution-based fabrication of flexible light-emitting device at ambient conditions. *J. Phys. Chem. C* **2013**, *117*, 16632−16639.

(26) Shin, J. H.; Matyba, P.; Robinson, N. D.; Edman, L. The influence of electrodes on the performance of light-emitting electrochemical cells. *Electrochim. Acta* **2007**, *52*, 6456−6462.
(27) Fang, J.; Matyba, P.; Robinson, N. D.; Edman, L. Identifying and alleviating electrochemical side-reactions in light-emitting electrochemical cells. *J. Am. Chem. Soc.* **2008**, *130*, 4562−4568.
(28) Fang, J.; Matyba, P.; Edman, L. The design and realization of flexible, long-lived light-emitting electrochemical cells. *Adv. Funct. Mater.* **2009**, *19*, 2671−2676.
(29) Li, X.; Gao, J.; Liu, G. Reversible luminance decay in polymer light-emitting electrochemical cells. *Appl. Phys. Lett.* **2013**, *102*, 223303.
(30) Meier, S. B.; Hartmann, D.; Tordera, D.; Bolink, H. J.; Winnacker, A.; Sarfert, W. Dynamic doping and degradation in sandwich-type light-emitting electrochemical cells. *Phys. Chem. Chem. Phys.* **2012**, *14*, 10886−10890.
(31) Shavaleev, N. M.; Scopelliti, R.; Gratzel, M.; Nazeeruddin, M. K.; Pertegas, A.; Roldan-Carmona, C.; Tordera, D.; Bolink, H. J. Pulsed-current versus constant-voltage light-emitting electrochemical cells with trifluoromethyl-substituted cationic iridium(III) complexes. *J. Mater. Chem. C* **2013**, *1*, 2241−2248.
(32) Tordera, D.; Meier, S.; Lenes, M.; Costa, R. D.; Orti, E.; Sarfert, W.; Bolink, H. J. Simple, fast, bright, and stable light sources. *Adv. Mater.* **2012**, *24*, 897−900.
(33) Tang, S.; Edman, L. Quest for an appropriate electrolyte for high-performance light-emitting electrochemical cells. *J. Phys. Chem. Lett.* **2010**, *1*, 2727−2732.
(34) Tordera, D.; Pertegas, A.; Shavaleev, N. M.; Scopelliti, R.; Orti, E.; Bolink, H. J.; Baranoff, E.; Gratzel, M.; Nazeeruddin, M. K. Efficient orange light-emitting electrochemical cells. *J. Mater. Chem.* **2012**, *22*, 19264−19268.
(35) Wenzl, F. P.; Pachler, P.; List, E. J. W.; Somitsch, D.; Knoll, P.; Patil, S.; Guentner, R.; Scherf, U.; Leising, G. Self-absorption effects in a LEC with low Stokes shift. *Physica E* **2002**, *13*, 1251−1254.
(36) Patil, A. O.; Heeger, A. J.; Wudl, F. Optical-Properties of Conducting Polymers. *Chem. Rev.* **1988**, *88*, 183−200.
(37) Tseng, C. Y.; Hu, C. W.; Huang, K. C.; Chang, L. C.; Vittal, R.; Ho, K. C. Ion transport across the film of poly(5,6-dimethoxyindole-2-carboxylic acid) in relation to its electrochromic switching: An electrochemical quartz crystal microbalance study. *Electrochim. Acta* **2013**, *101*, 232−237.
(38) Fang, J. F.; Yang, Y. L.; Edman, L. Understanding the operation of light-emitting electrochemical cells. *Appl. Phys. Lett.* **2008**, *93*, 063503.
(39) van Reenen, S.; Matyba, P.; Dzwilewski, A.; Janssen, R. A. J.; Edman, L.; Kemerink, M. Salt concentration effects in planar light-emitting electrochemical cells. *Adv. Funct. Mater.* **2011**, *21*, 1795−1802.
(40) Sandstrom, A.; Matyba, P.; Edman, L. Yellow-green light-emitting electrochemical cells with long lifetime and high efficiency. *Appl. Phys. Lett.* **2010**, *96*, 053303.
(41) Onoda, M.; Manda, Y.; Iwasa, T.; Nakayama, H.; Amakawa, K.; Yoshino, K. Electrical, optical, and magnetic-properties of poly(2,5-diethoxy-*para*-phenylene vinylene). *Phys. Rev. B* **1990**, *42*, 11826−11832.
(42) Onoda, M.; Morita, S.; Iwasa, T.; Nakayama, H.; Amakawa, K.; Yoshino, K. In situ absorption-spectra measurements in poly(1,4-naphthalene vinylene) during electrochemical doping. *J. Phys. D: Appl. Phys.* **1991**, *24*, 1152−1157.
(43) Holt, A. L.; Leger, J. M.; Carter, S. A. Electrochemical and optical characterization of p- and n-doped poly[2-methoxy-5-(2-ethylhexyloxy)-1,4-phenylenevinylene]. *J. Chem. Phys.* **2005**, *123*, 044704.
(44) Leger, J. M.; Carter, S. A.; Ruhstaller, B. Recombination profiles in poly[2-methoxy-5-(2-ethylhexyloxy)-1,4-phenylenevinylene] light-emitting electrochemical cells. *J. Appl. Phys.* **2005**, *98*, 124907.
(45) Shin, J. H.; Dzwilewski, A.; Iwasiewicz, A.; Xiao, S.; Fransson, A.; Ankah, G. N.; Edman, L. Light emission at 5 V from a polymer device with a millimeter-sized interelectrode gap. *Appl. Phys. Lett.* **2006**, *89*, 013509.
(46) Alem, S.; Gao, J. The effect of annealing/quenching on the performance of polymer light-emitting electrochemical cells. *Org. Electron.* **2008**, *9*, 347−354.
(47) Shin, J. H.; Robinson, N. D.; Xiao, S.; Edman, L. Polymer light-emitting electrochemical cells: Doping concentration, emission-zone position, and turn-on time. *Adv. Funct. Mater.* **2007**, *17*, 1807−1813.
(48) Tang, S.; Sandstrom, A.; Fang, J. F.; Edman, L. A solution-processed trilayer electrochemical device: Localizing the light emission for optimized performance. *J. Am. Chem. Soc.* **2012**, *134*, 14050−14055.
(49) Su, H. C.; Chen, H. F.; Chen, P. H.; Lin, S. W.; Liao, C. T.; Wong, K. T. Efficient solid-state white light-emitting electrochemical cells based on phosphorescent sensitization. *J. Mater. Chem.* **2012**, *22*, 22998−23004.
(50) Gambino, S.; Bansal, A. K.; Samuel, I. D. W. Photophysical and charge-transporting properties of the copolymer Super Yellow. *Org. Electron.* **2013**, *14*, 1980−1987.
(51) Asadpoordarvish, A.; Sandström, A.; Tang, S.; Granström, J.; Edman, L. Encapsulating light-emitting electrochemical cells for improved performance. *Appl. Phys. Lett.* **2012**, *100*, 193508.